RESEARCH



Impact of Nanocellulose Loading on the Crystal Structure, Morphology and Properties of PVDF/Magnetite@NC/BaTiO₃ Multi-component Hybrid Ceramic/Polymer Composite Material

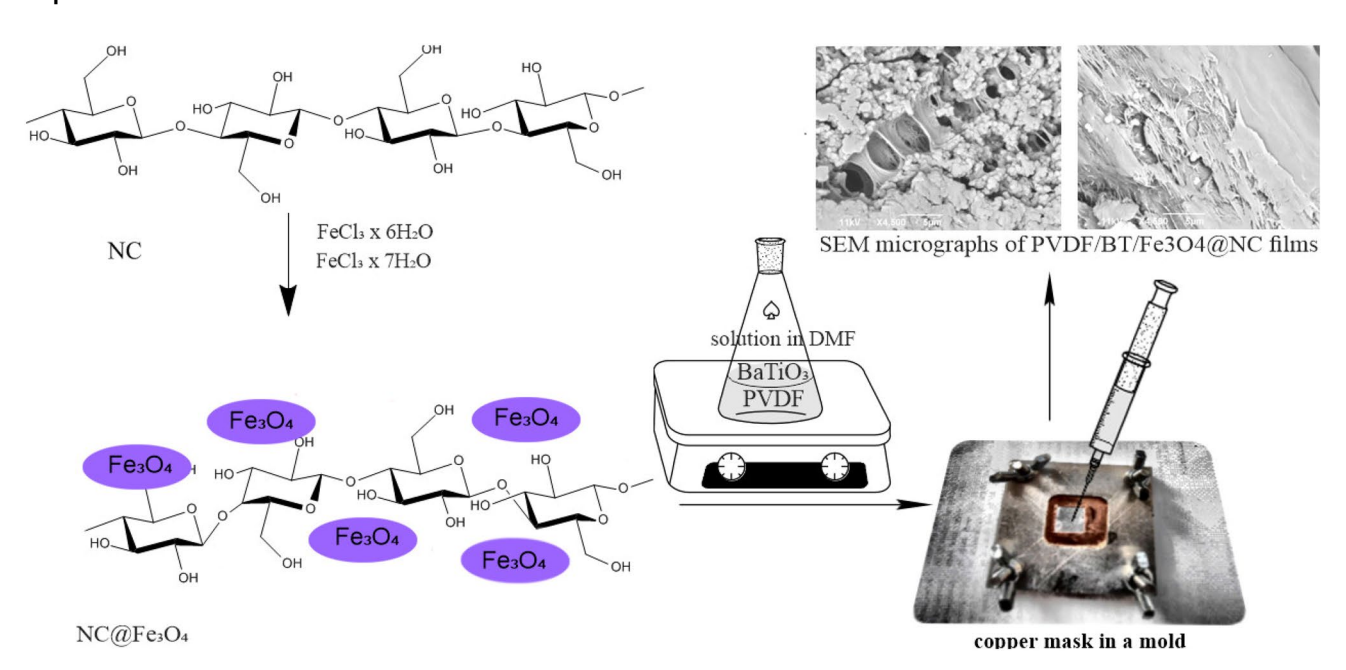
Aleksandra Janićijević¹ · Vera P. Pavlović² · Danijela Kovačević¹ · Nenad Đorđević¹ · Aleksandar Marinković³ · Branislav Vlahović^{4,5} · Abdennaceur Karoui⁴ · Vladimir B. Pavlović⁶ · Suzana Filipović⁷

Received: 11 April 2023 / Accepted: 20 November 2023 © The Author(s), under exclusive licence to Springer Science+Business Media, LLC, part of Springer Nature 2023

Abstract

The hybrid multifunctional magnetic organic/inorganic composite materials, with addition of optimal filler type and quantities are attractive due to wide range of potential application, from various pressure sensors, through smart packaging, to tissue engineering and medicine. The structural, morphological and magnetic properties of polyvinylidene fluoride/nanocellulose/magnetite@BaTiO₃ hybrid films were investigated. The presented study revealed significant impact of nanocellulose (NC) content on formation of the polymorphs of PVDF, responsible for ferro-, piezo- and pyroelectric properties. The structural characterization, XRD and Raman measurements confirmed enhancement of the β and γ phases when the loading of NC higher then 4 wt% in multi-component hybrid films. The saturation magnetization value gradually raises with increasing amount of NC and reaches its maximum value of 41.2 emu/g at content of 4 wt% NC. Further, addition of NC decreases saturation magnetization value regardless of constant amount of magnetite, indicating optimal content of NC substrate for co-precipitation of Fe₃O₄ onto NC matrix.

Graphical Abstract



Keywords Hybrid composites · Nanocellulose · Fe₃O₄ functionalization · PVDF · Magnetic properties

Extended author information available on the last page of the article

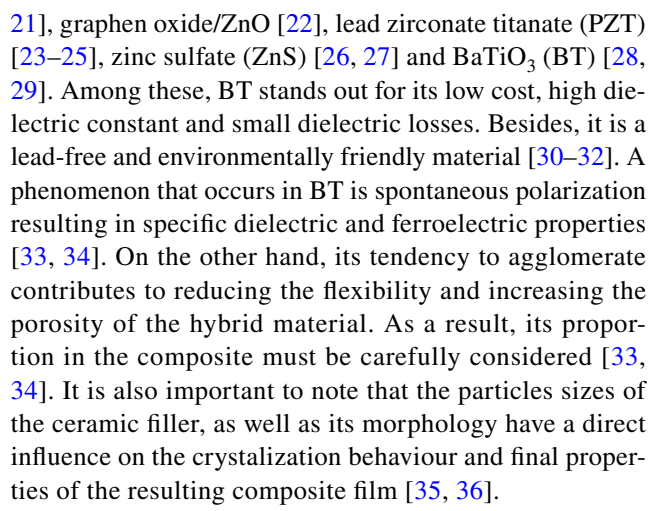
Published online: 29 November 2023



1 Introduction

The development of smart hybrid multifunctional magnetic organic/inorganic composite materials, with addition of optimal filler type and quantities, attracts great attention in the scientific community. Studies of hybrid materials based on polymers and ceramics filler have given interesting results in improvement of magnetic and electrical properties through prevention of mutual inhibition between different fillers and promotion of compatibility at the matrix/added components interface [1, 2]. The inclusion of the nanoparticles to the standard polymer matrix significantly improves properties of composites [3]. This way, materials of a wide range of applications could be obtained, from various pressure sensors, self-powered devices, through smart packaging, to tissue engineering and medicine [4-9]. Composites whose structure is of organic-inorganic origin are the most common, where the properties of the organic and inorganic precursors differ in the most aspects. Such a combination of the organic/ inorganic components creates a hybrid multifunctional material. High toughness, transparency, low weight, poor thermal conductivity, resistance to acids, alkalies, corrosion and water are the basic features of polymers [10, 11]. In combination with inorganic phases, mostly ceramic components, the range of properties expands by improving electrical and magnetic features [12, 13]. Special class of composites are multifferoic materials where more then one order states coexists, such as ferro-, magnetic and piezo. If properly connected, these phases can generate magnetoelectric (ME) strain, by which the exposure of the composite to the electric field can induce magnetic or piezo respond, and vice versa [14]. Such materials are highly usable as various sensors, actuators, transducers, etc.

Commonly used polymer is a polyvinylidene fluoride (PVDF). PVDF belongs to the semi-crystalline group of a non-toxic polymers. The strongly polar β -phase has the best piezoelectric and ferroelectric properties, while the most common and thermodynamically favorable α -phase is non-polar. The phases γ - and δ - appear to be weakly polar [15, 16]. Quenching and co-polymerization can induce a β- phase formation in the PVDF, but the most efficient mechanism appears to be addition of ceramic fillers [17, 18]. Ceramic fillers combined with ferroelectric polymers have a significant contribution in expansion of material potential application. Researchers have shown that ceramic fillers trigger crystallization of electro and magnetically active phases in polymers that have multiple crystalline phases. For piezoelectric polymer, ceramic fillers enhance the effect of converting mechanical energy into electrical (and vice versa) [19]. The successfully used ceramic fillers for the modification of the PVDF are zinc oxide (ZnO) [20,



Nanocelullose (NC) has piezo- nature and as a filler can give exceptional performance to the hybrid composite, which is reflected in mechanical strength, flexibility and dielectric properties [37–39]. Addition of the cellulose nanofiber into PVA, PLGA or PLA, acts as reinforcing agent which improves mechanical and barrier properties of the polymer films [40]. The interactions of OH groups (originated from NC) with fluorine in PVDF showed increase of β -PVDF phase formation. Studies have also shown that the size effects and the degree of crystallinity affect alpha to beta phase transformation of the PVDF [41, 42]. Several research groups determinate that exposure of the NC to magnetic field causes orientation of cellulose in a suspension [43]. Several routs were used to tailor crystallization direction in PVDF, such as mechanical activation or surface modification of filler particles [33]. The fillers surface modification has been shown as efficient way to improve interface compatibility between inorganic particles and organic matrix [36, 44]. Cellulose fibers modified by paramagnetic elements (deposition of iron) enable further improvement in cellulose orientation in a polymer matrix when exposed to lower strength of electric and magnetic fields [45]. Mix of magnetic, ferroelectric and piezo particles can give interesting results in terms of magnetic and electrical properties of the formed multiferroic hybrid composite materials if phases are well connected.

In this study, polyvinylidene fluoride (PVDF) was used as a matrix for synthesis of novel multi-component hybrid composite materials with a NC and BT as fillers for the first time, to the best of our knowledge. The effect of the NC content-surface modified with Fe_3O_4 , in presence of the ferroelectric (BT) phases, on PVDF crystallization behavior and magnetic properties was investigated. Barium titanate and nanocellulose (NC) functionalized with nanosized Fe_3O_4 were added as fillers into PVDF polymer matrix. The samples were prepared in the form of thick free-standing films, with thickness of a few tens of micrometers and area of 1 cm².



2 Experimental

2.1 Materials

The materials used in this paper were: commercially available cellulose, acetone (Sigma-Aldrich, p.a.), NN-dimethylformamide (DMF) (Sigma-Aldrich, p.a.), $FeSO_4 \times 7H_2O$ (Merck, p.a.), $FeCl_3 \times 6H_2O$ (Merck, p.a.), PVDF (homopolymer powder, SOLEF 1015/1001). NC washing, aqueous solution preparation and dish washing were all done with deionized water (DW) with a resistivity of $18~M\Omega$ cm. Concentration of PVDF solution and loading of Fe_3O_4 (4 wt%) and $BaTiO_3$ (4 wt%) were constant; only amount of NC was varied (1 wt%, 2 wt%, 4 wt%, 8 wt%) in a final multi-component composite materials.

2.2 Preparation of NC/Fe₃O₄

The preparation of the NC/Fe $_3O_4$ composite was explained in detail in previous work [46]. The acid hydrolysis (H $_2$ SO $_4$) of commercially available cellulose was applied to make nanocellulose (NC) according to a standard technique [47]. Ferri- and ferro- ions were co-precipitated in aqueous solution containing NC by addition of the ammonia to produce functionalized nanocellulose. Different concentrations of NC were used. The weight ratio of NC in Fe $_3$ O $_4$ /NC composites were 1:0.25; 1:0.5; 1:1; 1:2. The obtained slurry NC@Fe $_3$ O $_4$ were washed with distilled water and ethanol, and eventually dried.

According to the NC weight ratio in Fe₃O₄@NC composites the samples were labeled as: 1:0.25 (Fe₃O₄@NC1), 1:0.5 (Fe₃O₄@NC2), 1:1 (Fe₃O₄@NC4), 1:2 (Fe₃O₄@NC8).

2.3 Preparation of Multi-component Composites NC/Fe₃O₄/BaTiO₃/PVDF

PVDF (homopolymer powder, SOLEF 1015/1001) was firstly dissolved in a mixture of acetone/DMF (1:1) to obtain 20 wt% solution of polymer. BaTiO₃ (Sigma-Aldrich) was sonicated in DMF for 30 min and added to the dissolved polymer in an amount of 4 wt% with respect to the PVDF content. This mixture was stirred for 6 h to obtain

homogeneous BaTiO₃ dispersion. NC@Fe₃O₄ composites, with different content of NC, were sonicated in DMF for 30 min and subsequently added to PVDF/BaTiO₃ mixture, resulting in multi-component mixtures with four different concentrations of NC. To ensure adequate filler distribution inside the polymer matrix, the composites were agitated overnight at room temperature.

2.4 Film Preparation

The films were prepared by solution casting technique, using copper mask placed in a mold. Aluminum foil was first placed in a mold to provide an easy removal of the films from a copper mask. The copper mask, thickness of $100~\mu m$, was put over the aluminum foil and the mold system was fixed to prevent solvent leakage. After solvent evaporation the films were removed from the molds, separated from the copper mask and aluminum foil, dried for 5 days at room temperature and 8 h at $60~^{\circ} C$ in a vacuum oven. The prolonged drying process was applied in order to completely remove residue of the solvent, avoiding significant increase of temperature. It was done to avoid phase transition of the BaTiO₃ which can occur between 80 and $120~^{\circ} C$. The list of the samples is presented in the Table 1.

2.5 Characterization Techniques

The all of the samples were characterize at room temperature by X-ray diffraction (XRD) method using a BRUKER D8 ADVANCE with Vario 1 focusing primary monochromator (Cu $k_{\alpha 1}$ radiation, $\lambda = 1.54059$ Å). XRD patterns were collected in the Bragg's angle (2 θ) range of 10–90°.

In addition, the samples were measured using a Kratos Axis Ultra XPS system with Monochromated Aluminum K-Alpha X-Rays. The vacuum chamber during measurement was at 2.5×10^{-8} torr. The X-Ray gun was operated at 15 kW and 10 mA. A charge neutralizer was used to reduce charging effects from non-conducting surfaces. Electrons were collected at 90 degrees from the sample surface. All survey scans were collected with a Pass Energy of 160 eV and 1 sweep (or averaging). All Region scans were performed with a Pass Energy of 20 eV, and the number of sweeps (averages) performed was 5–6 sweeps, dependently on the region.

Table 1 The list of the film samples

| Samples | Polymer | wt% of BT | wt% of Fe ₃ O ₄ | wt% of NC | Mass fractions in hybrid composite PVDF/BT/ Fe ₃ O ₄ @NC |
|---|---------|-----------|---------------------------------------|-----------|--|
| PVDF/BT/Fe ₃ O ₄ @NC1 | PVDF | 4 | 4 | 1 | 91/4/5 |
| PVDF/BT/Fe ₃ O ₄ @NC2 | | | | 2 | 90/4/6 |
| PVDF/BT/Fe ₃ O ₄ @NC4 | | | | 4 | 88/4/8 |
| $PVDF/BT/Fe_3O_4@NC8$ | | | | 8 | 84/4/12 |



SEM (JSM-6390 LV scanning electron microscope, coupled with EDS Oxford Instruments X-MaxN) was used to analyze the morphology of the final composite films. Prior to measurements, the composite films were cryo-fractured in liquid nitrogen. Samples were covered with gold. The measurements were performed at room temperature.

Raman scattering was recorded using a Horiba Jobin Yvon LabRam ARAMIS system in a backscattering geometry. Unpolarized light scattering spectra of hybrid composite films were obtained at room temperature. As a source of excitation He–Ne laser with the 632.8 nm line, with the acquisition of 10s/5 cycles and with the power of 1 mW at the sample was used. The measurements were performed in range of 100–1600 cm⁻¹.

Magnetic measurements were performed using superconducting quantum interference device (SQUID) with a vibrating sample magnetometer (VSM) from Quantum Design. The samples were measured at room temperature with magnetic field up to ± 4.5 Tesla. Peak VSM amplitude of 5 mm with 2 s averaging time was used to improve measurement precision, especially around zero magnetization. Before measuring, the magnet was oscillated from 7 to 0 T to minimize flux pining.

3 Results and Discusion

The phase composition of the PVDF based composite films is investigated by XRD analysis. In X-ray diffractograms of composite films, presented in Fig. 1, the most evident signals originate from PVDF matrix and BT. All XRD peaks, characteristic for barium-titanate are present and clearly expressed (JCPDS Card No. 5-626). The asymmetry of BT peak at 2θ of 45.5°, which occurs due to diffraction in planes 002 and 200, confirms the tetragonal structure of barium titanate [48]. The peaks at higher Bragg's angles (in the region from 50° to 85°) also belong to the diffractions from barium titanate planes. The strongest line of nanocellulose emerges as a shoulder at 22.5° in diffraction pattern of the composite PVDF/BT/Fe₃O₄@NC8. No signals originating from Fe₃O₄ were detected. The low content of the Fe₃O₄ phase along with nano sized dimensions and the most likely amorphous structure cause failure to appear this phase in XRD patterns. The additional increase in the crystallite size would have beneficial effect on its appearance in the XRD patterns, but then it would influence the magnetic properties of the hybrid film. The XRD patterns of the Fe₃O₄@ NC composites were previously shown [45], and the results revile change in nanocellulose structure from cellulose II to cellulose I after Fe₃O₄ functionalization. The decrease in peaks intensity of the magnetite phase is also detected due to overall increase in the NC content within Fe₃O₄@NC1 to Fe₃O₄@NC8 samples. Some of the NC diffraction peaks

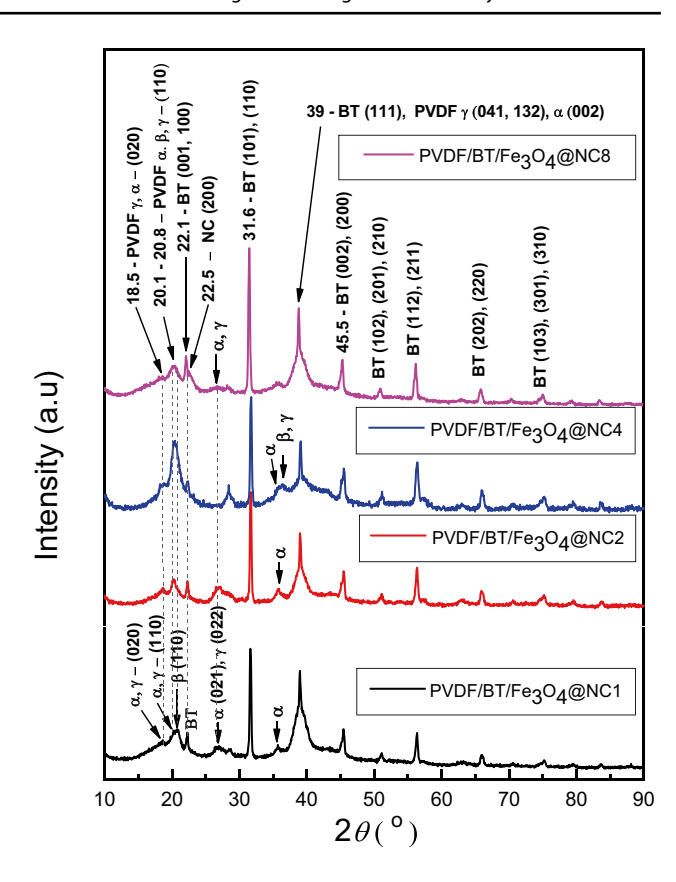


Fig. 1 Diffractograms of hybrid composite films. Labels α , β and γ refer to PVDF crystal phases. Label BT stands for barium titanate

are also shifted due to interaction between the composite constituents.

Among the PVDF peaks, those at 18.5° and 26.2° correspond to overlapped diffractions of α and γ crystalline phases of PVDF (JCPDS Cards No. 42-1650 and 38-1638), while the peak at $\sim 39^\circ$ includes an additional contribution of barium titanate (111) diffraction line. Although the strongest lines of α , β and γ crystalline phases of PVDF overlap forming the broad peak in the range of 20.1–20.8°, it is possible to notice the contribution of β (110) line at 20.7°, in the PVDF/BT/Fe₃O₄@NC1 sample (JCPDS Cards No.43-1650, 42-1649 and 38-1638). The peaks at ~ 26.5 –27.3° and $\sim 35.7^\circ$ originate dominantly from α phase [49–52], although the γ phase may give some contribution.

The phase composition of PVDF matrix was found to be influenced by the presence of nanocellulose. Namely, it can be noticed that the signals related dominantly to α phase, as well as to mutual contribution of α and γ phases, are of higher intensity in diffractogram of the sample containing 2 wt% of NC, comparing with those in composite sample loaded with 1 wt% of NC, indicating that higher amount of NC increases the content of α phase in PVDF matrix. Furthermore, the peak in the range of 20.1–20.8° shifts toward lower values of 2θ , which confirms the observation



of increasing amount of α and/or γ phase. According to diffractogram of the PVDF/BT/Fe $_3$ O $_4$ @NC8 sample, it seems that the further increase of NC content may lead to opposite effect, which results in lower amount of alpha phase in the PVDF matrix of composite, even when compared to PVDF/BT/Fe $_3$ O $_4$ @NC1 sample. However, the overlapping of the main XRD lines of PVDF blurs the precise conclusion. For that reason, Raman spectroscopy were performed in order to provide further insight in structural properties of multicomponent PVDF based composite films.

Raman spectra of all prepared samples are presented in Fig. 2. The broad Raman peaks in the regions around 270 and 520 cm⁻¹ are assigned to barium titanate $A_1(2TO)$ mode and $E(4TO) + A_1(3TO)$ modes respectively [48, 53, 54], even though these signals are partially overlapped by some of PVDF modes. The sharp peak at 306 cm⁻¹, corresponding to the tetragonal phase of barium titanate, is

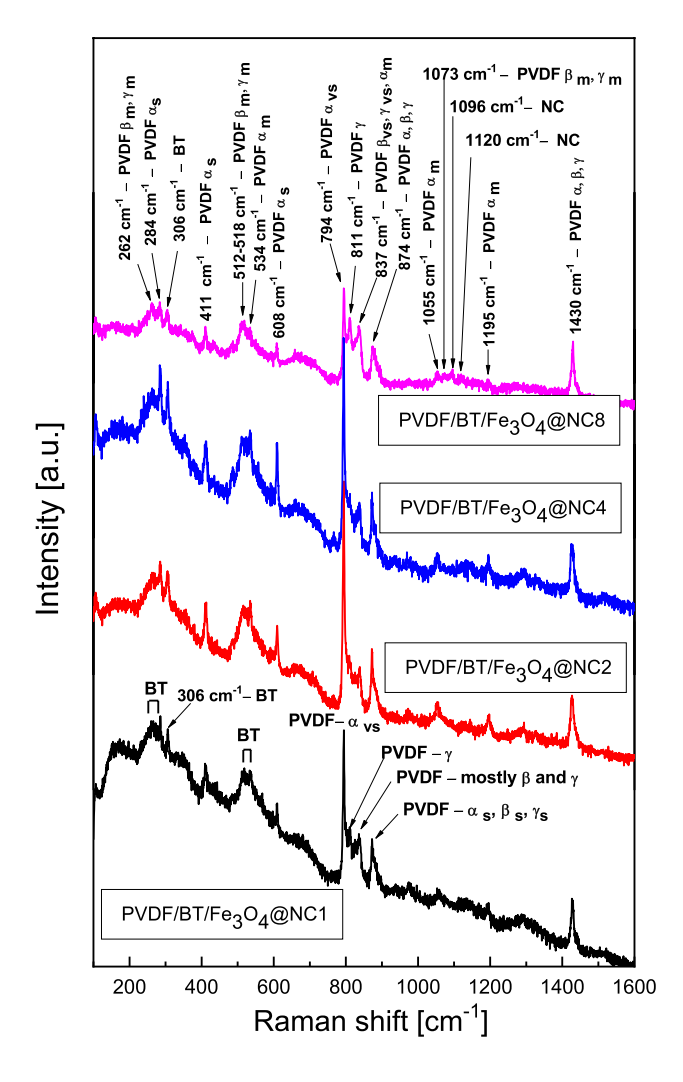


Fig. 2 Raman spectra of the multi-component composite films. Labels vs., s and m correspond to very strong, strong and medium intensity of the Raman lines in the pure spectrum of each of the observed PVDF crystalline phases

observed in all four spectra and those results are in accordance with results obtained from XRD analysis.

The composite sample loaded with 1 wt% of NC shows the presence of three crystalline phases of PVDF: α , β and γ , but it can be concluded that the most prevalent is the alpha form, considering that α line at 794 cm⁻¹ (the strongest alpha line, α_{vs} , in the pure alpha phase of PVDF) dominates the spectrum [55-58]. Increase in amount of NC from 1 to 2 wt% leads to even higher intensity of α line at 794 cm⁻¹, comparing to characteristic γ peak at 811 cm⁻¹, or to peak which mostly originates from beta and gamma phases at 837 cm⁻¹ [57, 59, 60]. A rise in intensity of strong alpha lines (α_s) at 411 cm⁻¹, 608 cm⁻¹ and 284 cm⁻¹, as well as medium alpha lines ($\alpha_{\rm m}$) at 534, 1055 and 1195 cm⁻¹, is also observed [56, 59, 59, 60]. These results indicate that that mentioned increase of NC amount causes the increase of α -phase of PVDF. The composite containing 4 wt% of nanocellulose demonstrated similar intensity of alpha lines, compared with the spectra of the composite having lower loading of NC (2 wt%), but the slight increase in intensity of the signal at 811 cm⁻¹ (contribution of γ phase) and at 837 cm⁻¹ (dominant contribution of β and γ phases) is noticed. The addition of 8 wt% of NC led to substantial increase in percentage of both β and γ phase, relative to all other samples (with lower contents of NC), which is proven via the changes in relative intensity of the lines in the region from 750 to 900 cm⁻¹. Namely, the conversion of α phase to β and γ is confirmed by decrease in intensity of very strong α line at 794 cm⁻¹ and by increase in the intensity of the lines at 811 and 837 cm⁻¹. Attenuation of the intensity of all lines attributed to the α phase, relative to the intensity of the peaks at 262 cm⁻¹, 512-518 cm⁻¹ and 1073 cm⁻¹ which originated from medium β and γ lines (β_m, γ_m) , also suggests transformation toward β and γ phase [56], induced by the higher amount of NC. The Raman signals at 1096 and 1120 cm⁻¹, characteristic for NC, become evident when the highest percentage of NC is added to PVDF based composite material. Even then, the signals of NC are less pronounced, comparing with dominant signals of the polymer matrix [56]. The Raman signals at 1096 and 1120 cm⁻¹, characteristic for NC, become evident when the highest percentage of NC is added to PVDF based composite material. Even then, the signals of NC are less pronounced, comparing with dominant signals of the polymer matrix [57]. Increase in NC content over 2 wt% triggers crystallization of the PVDF in the electrically most favorable β phase, through increasing in interactions of OH groups (originated from NC) with fluorine in PVDF [41, 42]. The increase in conversion from α to β phase was also noted when surface fluorinated nanocellulose was added to the PVDF matrix due to better connectivity between phases when the NC is surface modified [60]. These films showed increased sensitivity comparing to pure PVDF. On the other hand, some of the research have shown reduced effect of



the different loading of the modified BT particles and/or surface modified NC addition on crystal structure or lattice vibrations, but significant increase in Young modulus [36].

Figure 3 presents XPS wide scan spectra of PVDF based composite films with different loading of NC. C 1s signal, originating from PVDF and NC, F 1s and F 2s signals from PVDF matrix, as well as O 1s signal obtained from NC/Fe₃O₄ and BaTiO₃, can be observed in the figure.

Figure 3 shows the C 1s core level scan spectra of the multi component composite films. These spectra were curve-fitted with five peak components, assigned to C–H species, CH₂, C–O and O–C–O/C=O species, CF₂ and –HC=CF– species. The peaks with binding energies (BEs) at \sim 286.0 eV (CH₂) and \sim 290.5 eV (CF₂) are characteristic for PVDF matrix [61]. The integrated area ratio of these peaks was maintained close to 1 (between 1 and 1.1) during the fitting, which is consistent with the chemical structure of PVDF and the data reported in literature [62, 63]. Although the peak attributed to C–H species, at BE of \sim 284.5 eV, may occur in PVDF [62], its presence is more common in cellulosic materials. The existence of these non-oxidized

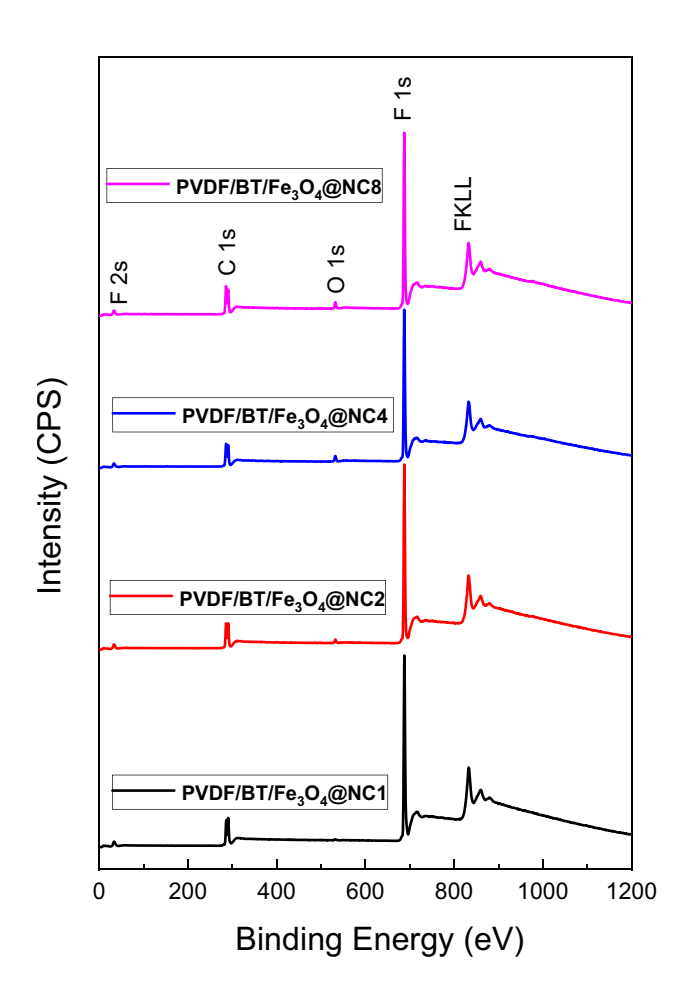


Fig. 3 Survey X-ray photo-electron spectra of the of PVDF based composite films

alkane-type carbon atoms is usually associated with the presence of residual lignin, extractive substances and fatty acids [64]. In the Fig. 4, the most pronounced effect of increased loading of NC is the rise in intensity of the C–H peak.

The peak obtained at region 286.7–287.4 eV, after the fitting of spectra, originates dominantly from contribution of carbons bonded to one oxygen atom (C–O), and to a lower degree from carbons attached to two oxygen atoms or a carbonyl group (O–C–O, C=O). In pure cellulose, the region of 286.7–287.4 eV is rather intensive and can be deconvoluted in the C–O and O–C–O/C=O signals, which has been usually detected at 286.7 and 288.3 eV respectively, where the first signal is more pronounced [64]. In our spectra, it was observed that peak area of C–O signal slightly increases with growing content of NC.

It was reported that dehydrofluorination may happen in PVDF under basic conditions, causing the occurrence of unsaturated -HC=CF- bonds [65]. Thus, the peak obtained in region 291–292 eV, after the deconvolution, can be attributed to -HC=CF- group. As a result of the transformation of the chemical environment of F atoms from CH_2-CF_2 to -HC=CF-, a certain shift of F 1s peak of PVDF matrix to ~ 687.7 eV, was noticed in our spectra (Fig. 5b), since the PVDF generally has an F1s BE down to 686.4 eV. According to the intensity of F 1s peak, the fluorine content was

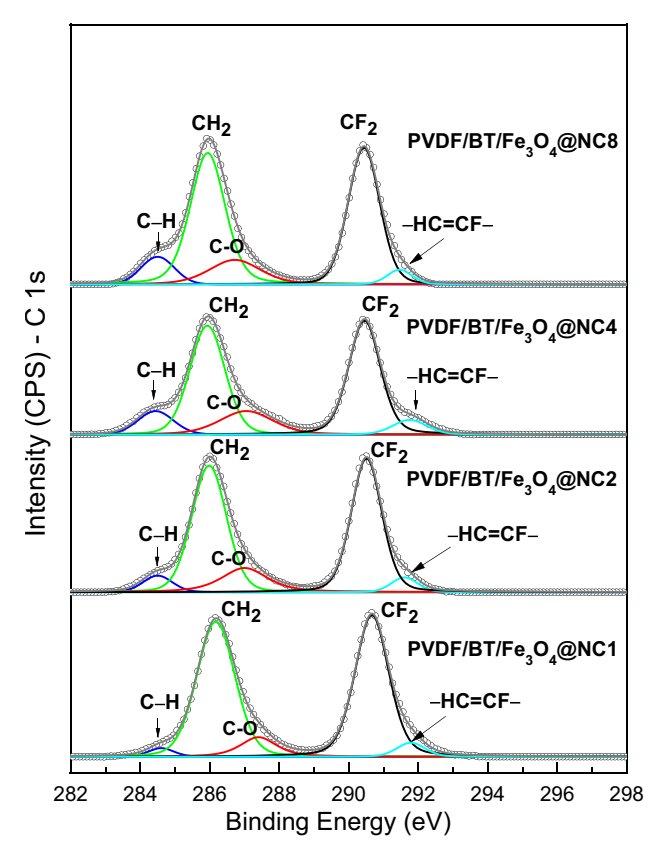


Fig. 4 XPS C 1s core-level spectra of PVDF based composite films



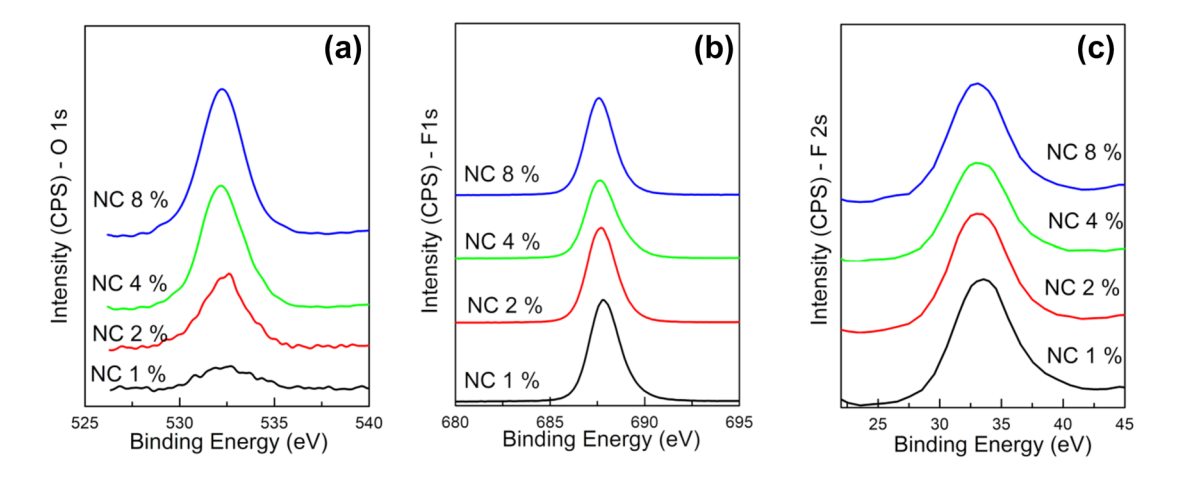


Fig. 5 High resolution XPS of the: a O 1s region, b F1s region and c F 2s region of the PVDF-based composite films

found to decrease until concentration of NC reached 4 wt%, while a change in this trend was observed when NC loading raised to 8 wt%. This conclusion was confirmed by The F 2s core-level spectra (Fig. 5c). It is also in accordance with observation that the intensity of the –HC=CF– peak slightly increases with loading of NC up to 4% (Fig. 4).

Oxygen content from O 1s core-level spectra (Fig. 5a) increased with increasing NC concentration, since NC contains numerous C–O and C=O functional groups.

Figure 6 shows the SEM micrographs of the cryo-fractured surfaces of composite samples with four different weight ratios of nanocellulose. The dispersed phase morphology influences and determines properties of polymer composites. The compatibility at the interface polymer matrix/dispersed phase defines phase morphology of the final products. The addition of several different fillers alerts structural and dimensional stability of PVDF matrix and is essential for enhancement of certain polymorph forms. The appropriate functionalization, i.e. compatible functional groups on the fillers surface can lead to a specific orientation of PVDF chains and to induce formation of desired phase, while at the same time stronger interface interaction between added particles and PVDF matrix can be establish.

The film containing 1 wt% of NC showed non-uniform structure with areas of agglomerated fillers on the surface of polymer matrix (Fig. 6a). Increased amount of NC (2 wt%) resulted in the more uniform morphology of the formed film, although non-uniform distribution of added components can be observed in the case of PVDF/BT/Fe₃O₄@NC2 composite, as well. The transformation in specific grain structure occurs when content of NC reaches 4 wt% and can be clearly seen in composite sample PVDF/BT/Fe₃O₄@NC4. The obtained results indicate that higher concentration of NC (4 wt%) contributes to formation of elongated micro fibrils at the composite surface. The formation of filament/fibrous structures, observed at fracture surface starts gradually in

the sample PVDF/BT/Fe₃O₄@NC4 and becomes the most evident in composite whit a NC loading of 8 wt%. The micro fibrils in the case of composite PVDF/BT/Fe₃O₄@NC8 become smaller, thinner and the complete polymer structure is more cohesive. The prevailing filament structure is responsible for uniform and smooth surface of the final composite sample when NC content reached its maximum.

A magnetic behavior of the hybrid composite PVDF-based films was also investigated. Comparative M–H curves recorded at room temperature for all four samples are presented in Fig. 7. Curvatures represent typical super-paramagnetic behavior for all samples. This means existence of very thin magnetic hysteresis loops, which can be detected only under magnification, as well as clear magnetic saturation under high magnetic field [66, 67].

Even though content of Fe_3O_4 is kept constant in all prepared composite films, the values of M_s show the differences and dependence on NC content. The value of saturation magnetization (M_c) was 35.9 emu/g in the sample PVDF/ BT/Fe₃O₄@NC1, then increased up to 39 emu/g for PVDF/ BT/Fe₃O₄@NC2, and finally reached its highest level of 41.2 emu/g for the composite film containing 4 wt% of NC. Saturation magnetization of the magnetite depends on preparation method, particle size and distribution and morphology. Within the agglomerated magnetic nanoprticles, such spatial arrangement has significant influence on net magnetization [66, 67]. Similar values of the saturation magnetization were achieved when the commercial Fe₃O₄ (5 nm) powder was dispersed directly into the PVDF matrix [68]. Although, the concentration of the magnetic phase was significantly higher. Not only that M_s has been improved by addition of the Fe₃O₄ phase to the PVDF matrix, the enhance in ferroelectric properties was also achieved through the interaction between the nanoparticles and the CH2 groups of the polymer chains [68]. Less aggregation of the individual magnetic particles, that is achieved in this paper by using



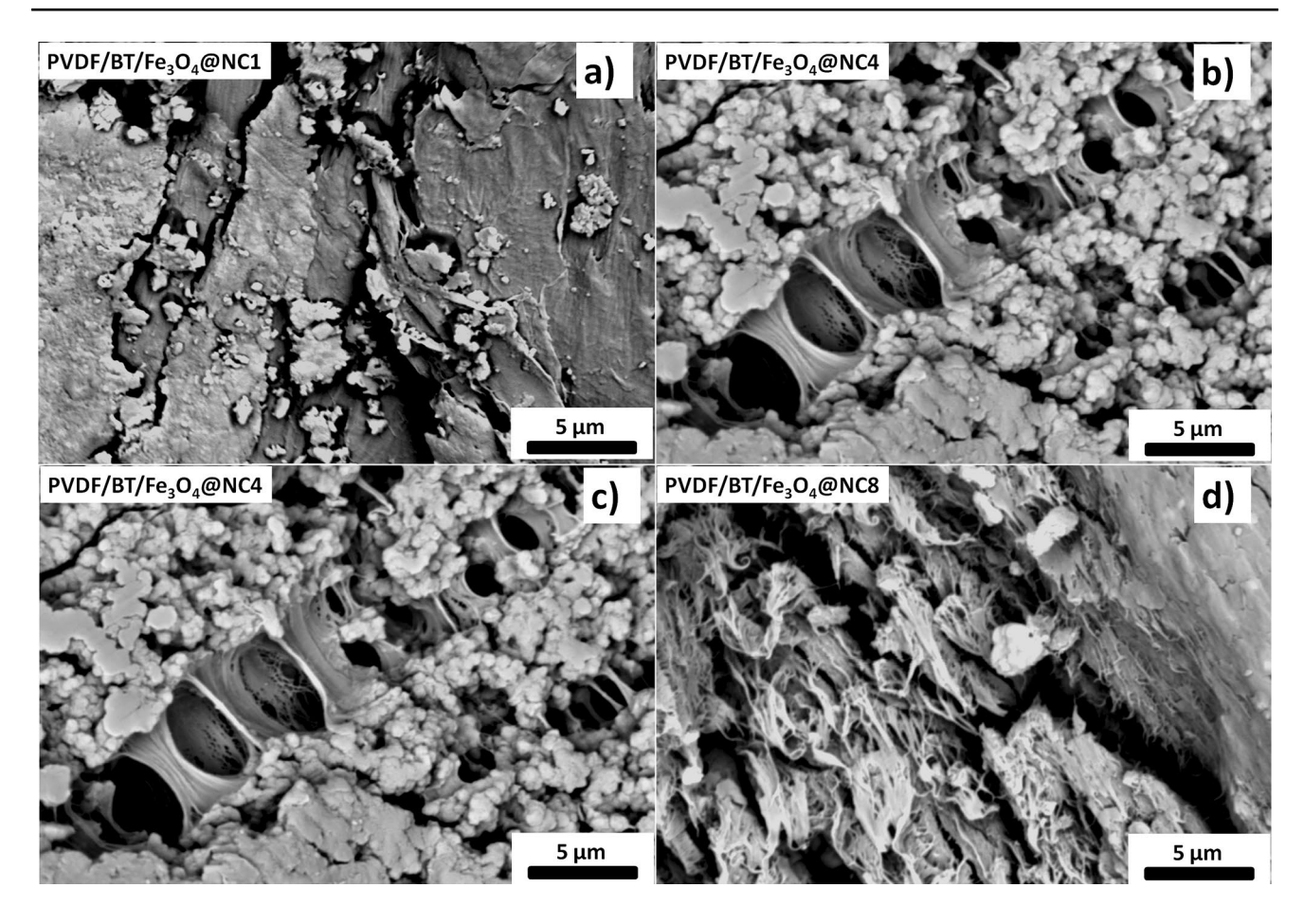


Fig. 6 SEM micrographs of the samples PVDF/BT/Fe₃O₄@NC with different loading of NC a 1 wt%, b 2 wt%, c 4 wt% and d 8 wt%

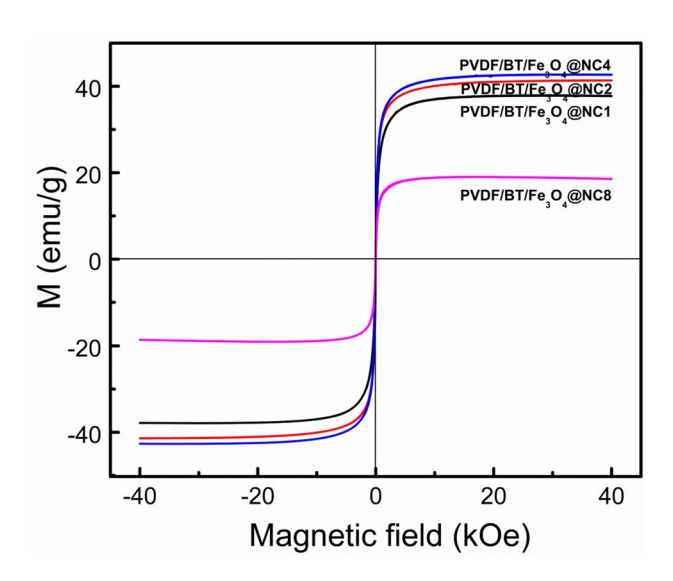


Fig. 7 Comparative magnetization curves

NC, proves to be beneficial to the improving M_s . As it has been shown in SEM images for samples PVDF/BT/Fe₃O₄@ NC1-PVDF/BT/Fe₃O₄@NC4 (Fig. 6a-c), the agglomeration of the magnetic particles on the surface of the polymer matrix decreases with increase of the NC amount up to 4 wt%. Thus, weaker interaction between Fe₃O₄ particles increases macroscopic magnetization, due to decrease in inter-particle dipolar forces [69]. Further addition of nanocellulose significantly reduced value of M_s at 18.9 emu/g. The PVDF, NC and BaTiO₃ are nonmagnetic components and the additional increase in the NC loading to 8 wt% takes over the dominant influence on saturation magnetization within sample PVDF/BT/Fe₃O₄@NC8. The decrease in magnetization per mass unit compared to bulk magnetite with the addition of a nonmagnetic component is in accordance with theoretical prediction and literature [70, 71]. The decrease in M_s would be expected for all additions of the NC higher then 1 wt%, due to rule of mixture, but as noted earlier in text, the optimal addition of NC leads to enhancement of the composite's performance for those NC concentrations due to better rearrangement and morphology of the films. It is evident that optimal amount of NC contributes to a higher



Table 2 Values of the coercive field and remnant magnetization for all hybrid composite films

| Sample | Hc [Oe] | Mr [emu/g] |
|--|---------|------------|
| PVDF/Fe ₃ O ₄ /NC1 | 28.5 | 2.72 |
| PVDF/Fe ₃ O ₄ /NC2 | 29 | 4.42 |
| PVDF/Fe ₃ O ₄ /NC4 | 28.3 | 4.24 |
| PVDF/Fe ₃ O ₄ /NC8 | 32 | 2.63 |

value of saturation magnetization, and magnetic properties of composite film may be tailored indirectly through the content of one component in multi-component hybrid composite material.

Although the values of the Hc and Mr, presented in Table 2, slightly fluctuate with NC content, the variations are not significant. The superparamagnetic behavior of the synthesized composites disables more precise measurements. The variation in amount of NC from 0.5 to 4 wt% for PDF-based composites wasn't give significant improvement in crystallinity or β -PVDF content, notwithstanding the linear trend was shown. The morphology of the obtained composite showed decrease in dimensions of the fibers up to 4 wt% of added NC [72]. These observations were in accordance with our results.

The final features of multi-component composite materials greatly depend on the properties of the each individual component, their mutual interaction and matrix-filler interaction. The addition of right type and amount of fillers in chosen matrix can result in material tailored to overcome some of the each components initial limitation. The obtained results in analysis of PVDF based multi-component hybrid material suggest different possibilities for film application by changing one component loading. Enhancement in content of the β -phase PVDF crystal structure and the most uniform morphology of the film was achieved with the highest loading of NC, while the best magnetic properties showed film having 4 wt% NC. From this it is possible to obtain films with precisely defined characteristics according to requirements by changing concentration of the one component in the multi component system. Since these materials have potential application as various sensors and actuators, due to their fast electromagnetic response, the PVDF/BT/Fe₃O₄@ NC4 film would be promising candidate.

4 Conclusion

The presented study investigated influence of nanocellulose amount on morphology development, crystallization behaviour and magnetic feature of multi-component hybrid composite materials based on PVDF polymer matrix. Fe₃O₄/ NC composites were integrated into a PVDF matrix with BaTiO₃ to create multi-component hybrid materials with different amounts of NC. The XRD, XPS and Raman analysis have been employed in order to determine influence of NC percentage on β -phase formation in PVDF matrix. NC also had impact on morphology of hybrid films in terms of transformation of prevailing grain structure with a small portion of elongated micro fibrils (for films up to 4 wt% of NC) to dominant filament/fibrous structure (8 wt% of NC). The magnetic behavior of prepared hybrid films showed to be strongly influenced by content of NC. Namely, by optimizing the substrate surface area for Fe₃O₄ co-precipitation the optimal morphology for reducing inter-particle interaction was achieved. Among examined samples, the highest value of saturation magnetization was obtained for composite film containing 4 wt% of NC, due to favorably developed microstructure for this sample.

Author Contributions AJ: Writing—Original Draft, Investigation; VPP: Formal analysis, Writing—Review & Editing, Visualization; DK: Resources, Investigation; NĐ: Writing—Review & Editing; AM: Supervision, Methodology; BV: Writing—Review & Editing, Supervision, Funding acquisition; AK.: Investigation, Funding acquisition; VBP:: Writing—Review & Editing, Supervision, Methodology, Project administration; SF: Writing—Review & Editing, Supervision, Visualization.

Funding This work was financially supported by the Ministry of Science, Technological Development and Innovation of the Republic of Serbia, through agreements related to the realization and financing of scientific research work at the Institute of Technical Sciences of SASA, Faculty of Agriculture of the University of Belgrade, Faculty of Mechanical Engineering of the University of Belgrade in 2023, Contract numbers: 451-03-47/2023-01/200175, 451-03-47/2023-01/200116, 451-03-47/2023-01/200105 as well as support for North Carolina Central University, award numbers: NSF DMR EiR 2101041, NSF DMR PREM 2122044, and DOE/NNSA NA0003979 and USA NSF PREM award DMR 2122044.

Declarations

Competing interest The authors declare no competing interests.

References

- H. Gu, C. Liu, J. Zhu, J. Gu, E.K. Wujcik, L. Shao, N. Wang, H. Wei, R. Scaffaro, J. Zhang, Z. Guo, Adv. Compos. Hybrid. Mater. 1, 1 (2018)
- J. Park, S.Y. Park, D. Lee, Y.S. Song, Smart Mater. Struct. 29, 055037 (2020)
- D. Aravind, K. Senthilkumar, M. Chandrasekar, T. Senthil Muthu Kumar, C. Ganesan, J. Parameswaranpillai, N. Rajini, S. Siengchin, N. Varagunapandiyan, Polym. Compos. 43, 6803 (2022)
- J. Kumar, R.K. Singh, S.B. Samanta, R.C. Rastogi, R. Singh, Macromol. Chem. Phys. 207, 1584 (2006)
- R. Gonçalves, P.M. Martins, C. Caparrós, P. Martins, M. Benelmekki, G. Botelho, S. Lanceros-Mendez, A. Lasheras, J. Gutiérrez, J.M. Barandiarán, J. Non-cryst. Sol. 361, 93 (2013)



- O.D. Jayakumar, B.P. Mandal, J. Majeed, G. Lawes, R. Naik, A.K. Tyagi, J. Mater. Chem. C 1, 3710 (2013)
- M. Shabanian, M. Khoobi, F. Hemati, H.A. Khonakdar, S. esmaeil, S. ebrahimi, U. Wagenknecht, A. Shafiee, J. Indust. Eng. Chem. 24, 211 (2015)
- 8. X. Huo, W. Li, J. Zhu, L. Li, Y. Li, L. Luo, Y. Zhu, J. Phys. Chem. C 119, 25786 (2015)
- 9. C. Tsonos, N. Soin, G. Tomara, B. Yang, G.C. Psarras, A. Kanapitsas, E. Siores, RSC Adv. 6, 1919 (2015)
- V. Revathi, S. Dinesh Kumar, P. Chithra Lekha, V. Subramanian, T.S. Natarajan, C. Muthamizhchelvan, Acta Metall. Sin. (Engl. Lett.) 27, 557 (2014)
- D.A. Seanor, Electrical Properties of Polymers (Acadenic press, USA, 1982)
- H.-C. Yang, J. Hou, V. Chen, Z.-K. Xu, J. Mater. Chem. A 4, 9716 (2016)
- 13. P. Eltouby, I. Shyha, C. Li, J. Khaliq, Ceram. Int. 47, 17813 (2021)
- R.N.P. Behera, P.R. Choudhary, Das, J. Mater. Sci. Mater. Electron. 28, 2586 (2017)
- 15. L. Li, M. Zhang, M. Rong, W. Ruan, RSC Adv. 4, 3938 (2013)
- S. Barrau, A. Ferri, A. Da Costa, J. Defebvin, S. Leroy, R. Desfeux, J.-M. Lefebvre, ACS Appl. Mater. Interfaces 10, 13092 (2018)
- A. De Neef, C. Samuel, H. Amorin, G. Stoclet, R. Jimenez, P. Dubois, J. Soulestin, J.M. Raquez, ACS Appl. Polym. Mater. 2, 3766 (2020)
- Z. Yin, B. Tian, Q. Zhu, C. Duan, Polymers (Basel) 11, 2033 (2019)
- H. Kim, F. Torres, D. Villagran, C. Stewart, Y. Lin, T.-L.B. Tseng, Macromol. Mater. Eng. 302, 1700229 (2017)
- J. Li, C. Zhao, K. Xia, X. Liu, D. Li, J. Han, Appl. Surf. Sci. 463, 626 (2019)
- M.V. Arularasu, M. Harb, R. Vignesh, T.V. Rajendran, R. Sundaram, Surf. Interfaces 21, 100780 (2020)
- 22. B. Jaleh, A. Jabbari, Appl. Surf. Sci. 320, 339 (2014)
- X. Niu, W. Jia, S. Qian, J. Zhu, J. Zhang, X. Hou, J. Mu, W. Geng,
 J. Cho, J. He, X. Chou, ACS Sustain. Chem. Eng. 7, 979 (2019)
- M. Selvaraj, R. Senthilkumar, R. Balaji, S. Selvasekarapandian, T.G. Manivasagam, AIP Conf. Proc. 2162, 020056 (2019)
- J.E.Q. Quinsaat, T. de Wild, F.A. Nüesch, D. Damjanovic, R. Krämer, G. Schürch, D. Häfliger, F. Clemens, T. Sebastian, M. Dascalu, D.M. Opris, Compos. Part B Eng. 198, 108211 (2020)
- H. Li, Y. Zhang, H. Dai, W. Tong, Y. Zhou, J. Zhao, Q. An, Nanoscale 10, 5489 (2018)
- A. Sultana, M.M. Alam, S. Garain, T.K. Sinha, T.R. Middya, D. Mandal, ACS Appl. Mater. Interfaces 7, 19091 (2015)
- V.P. Pavlović, V.B. Pavlović, B. Vlahović, D.K. Božanić, J.D. Pajović, R. Dojčilović, V. Djoković, Phys. Scr. T157, 014006 (2013)
- J. Nunes-Pereira, V. Sencadas, V. Correia, V.F. Cardoso, W. Han, J.G. Rocha, S. Lanceros-Méndez, Compos. Part B Eng. 72, 130 (2015)
- H. Yang, Z. Lu, L. Li, W. Bao, H. Ji, J. Li, A. Feteira, F. Xu, Y. Zhang, H. Sun, Z. Huang, W. Lou, K. Song, S. Sun, G. Wang, D. Wang, I.M. Reaney, ACS Appl. Mater. Interfaces 12, 43942 (2020)
- G. Jian, Y. Jiao, Q. Meng, Y. Cao, Z. Zhou, K.S. Moon, C.P. Wong, J. Mater. Sci. 50, 6903 (2020)
- 32. R. Popielarz, C.K. Chiang, Mater. Sci. Eng. B 139, 48 (2007)
- T.G. Mofokeng, A.S. Luyt, V.P. Pavlović, V.B. Pavlović, D. Dudić,
 B. Vlahović, V. Djoković, J. Appl. Phys. 115, 084109 (2014)
- V.P. Pavlović, D. Tošić, R. Dojčilović, D. Dudić, M.D. Dramićanin, M. Mandić, M.M. McPherson, V.B. Pavlović, B. Vlahović, V. Djoković, Polym. Test 96, 107093 (2021)
- R. Zhang, L. Li, S. Long, Y. Shen, H. Lou, F. Wen, H. Hong, G. Wang, W. Wu, Cearm. Int. 476, 22155 (2021)

- F. Ram, P. Kaviraj, R. Pramanik, A. Krishnan, K. Shanmuganathan, A. Arockiarajan, J. Alloys Compd. 823, 153701 (2020)
- N. Đorđević, A.D. Marinković, J.B. Nikolić, S.Å. Drmanić, M. Rančić, D.V. Brković, P.S. Uskoković, J. Serb. Chem. Soc. 81, 589 (2016)
- H. Fashandi, M.M. Abolhasani, P. Sandoghdar, N. Zohdi, Q. Li, M. Naebe, Cellulose 23, 3625 (2016)
- Y.B.P. T, V. Bobnar, S. Gorgieva, Y. Grohens, M. Finšgar, S. Thomas, V. Kokol, RSC Adv. 6, 49138 (2016)
- S. Purkayastha, M. Prakash, A.K. Ghosh, S. Saha, Polym. Compos. 43, 6887 (2022)
- 41. J. Kim, S. Yun, Z. Ounaies, Macromolecules 39, 4202 (2006)
- 42. P.S.M. Rajesh, S. Bodkhe, S. Kamle, V. Verma, Electron. Mater. Lett. 10, 315 (2014)
- M. Tatsumi, F. Kimura, T. Kimura, Y. Teramoto, Y. Nishio, Biomacromolecules 15, 4579 (2014)
- Z.-M. Dang, H.-Y. Wang, H.-P. Xu, Appl. Phys. Lett. 89, 112902 (2006)
- 45. S.T. Sundar, M.M. Sain, K. Oksman, Carbohydr. Polym. **80**, 35
- A. Janićijević, V.P. Pavlović, D. Kovačević, M. Perić, B. Vlahović, V.B. Pavlović, S. Filipović, Polymers 14, 1819 (2022)
- 47. D. Bondeson, A. Mathew, K. Oksman, Cellulose 13, 171 (2006)
- 48. P. Zhu, L. Feng, Z. Ding, X. Bai, Int. J. Mol. Sci. 23, 10764 (2022)
- V. Tomer, E. Manias, C.A. Randall, J. Appl. Phys. 110, 044107 (2011)
- 50. W. Ma, J. Zhang, X. Wang, J. Mater. Sci. 43, 398 (2008)
- 51. W.A. Yee, M. Kotaki, Y. Liu, X. Lu, Polymer 48, 512 (2007)
- 52. R. Gregorio Jr., J. Appl. Polym. Sci. 100, 3272 (2006)
- H. Zhang, B. Cheng, Q. Li, B. Liu, Y. Mao, J. Phys. Chem. C 122, 5188 (2018)
- W. Han, J. Zhu, S. Zhang, H. Zhang, X. Wang, Q. Wang, C. Gao, C. Jin, J. Appl. Phys. 113, 193513 (2013)
- 55. P. Nallasamy, S. Mohan, IJPAP 11, 43 (2005)
- D. Chipara, V. Kuncser, K. Lozano, M. Alcoutlabi, E. Ibrahim, M. Chipara, J. Appl. Polym. Sci. 137, 48907 (2020)
- P. Sedlak, D. Sobola, A. Gajdos, R. Dallaev, A. Nebojsa, P. Kubersky, Polymers 13, 2678 (2021)
- Q. Wu, A. Tiraferri, T. Li, W. Xie, H. Chang, Y. Bai, B. Liu, ACS Omega 5, 23450 (2020)
- S. Satapathy, S. Pawar, P.K. Gupta, K.B.R. Varma, Bull. Mater. Sci. 34, 727 (2011)
- F. Ram, A. Gudadhe, T. Vijayakanth, S. Aherrao, V. Borkar, R. Boomishankar, K. Shanmuganathan, Appl. Polym. Mater. 2, 2550 (2020)
- U.P. Agarwal, R. Sabo, R.S. Reiner, C.M. Clemons, A.W. Rudie, Appl. Spect. 66, 750 (2012)
- T. Cai, R. Wang, K.G. Neoh, E.T. Kang, Polym. Chem. 2, 1849 (2011)
- G. Zhai, L. Ying, E.T. Kang, K.G. Neoh, J. Mater. Chem. 12, 3508 (2002)
- 64. K. Missoum, J. Bras, M.N. Belgacem, Cellulose 19, 1957 (2012)
- 65. K. Feng, B. Tang, P. Wu, J. Mater. Chem. A3, 12609 (2015)
- J. Guo, I. Filpponen, L.-S. Johansson, P. Mohammadi, M. Latikka, M.B. Linder, R.H.A. Ras, O.J. Rojas, Biomacromolecules 18, 898 (2017)
- 67. S. Azad, B.B.F. Mirjalili, RSC Adv. 6, 96928 (2016)
- 68. X. Gao, S. Liang, A. Ferri, W. Huang, D. Rouxel, X. Devaux, X.-G. Li, H. Yang, M. Chshiev, R. Desfeux, A. Da Costa, G. Hu, M. Stoffel, A. Nachawaty, C. Jiang, Z. Zeng, J.-P. Liu, H. Yang, Y. Lu, Appl. Phys. Lett. 116, 152905 (2020)
- M. Knobel, W.C. Nunes, L.M. Socolovsky, E. De Biasi, J.M. Vargas, J.C. Denardin, J. Nanosci. Nanotechnol. 8, 2836 (2008)
- N. Amiralian, M. Mustapic, M.S.A. Hossain, C. Wang, M. Konarova, J. Tang, J. Na, A. Khan, A. Rowan, J. Haz. Mater. 394, 122571 (2020)



- C.I. Covaliu, D. Berger, C. Matei, L. Diamandescu, E. Vasile, C. Cristea, V. Ionita, H. Iovu, J. Nanopart Res. 13, 6169 (2011)
- A. Issa, M. Al-Maadeed, A.S. Luyt, M. Mrlik, M.K. Hassan, J. Appl. Polym. Sci. 133, 43594 (2016)

Publisher's Note Springer Nature remains neutral with regard to jurisdictional claims in published maps and institutional affiliations.

Springer Nature or its licensor (e.g. a society or other partner) holds exclusive rights to this article under a publishing agreement with the author(s) or other rightsholder(s); author self-archiving of the accepted manuscript version of this article is solely governed by the terms of such publishing agreement and applicable law.

Authors and Affiliations

Aleksandra Janićijević¹ · Vera P. Pavlović² · Danijela Kovačević¹ · Nenad Đorđević¹ · Aleksandar Marinković³ · Branislav Vlahović^{4,5} · Abdennaceur Karoui⁴ · Vladimir B. Pavlović⁶ · Suzana Filipović⁷

- Suzana Filipović suzana.filipovic@itn.sanu.ac.rs
- The Academy of Applied Technical Studies Belgrade, Belgrade, Serbia
- Faculty of Mechanical Engineering, University of Belgrade, Belgrade, Serbia
- Faculty of Technology and Metallurgy, University of Belgrade, Belgrade, Serbia
- ⁴ North Carolina Central University, Durham, NC 27707, USA
- NASA University Research Center for Aerospace Device Research and Education and NSF Center of Research Excellence in Science and Technology Computational Center for Fundamental and Applied Science and Education, Durham, NC 27707, USA
- Department for Physics and Mathematics, Faculty of Agriculture, University of Belgrade, Belgrade, Serbia
- Institute of Technical Sciences of SASA, Kneza Mihaila 35/IV, Belgrade 11000, Serbia

